ORIGINAL PAPER

N. Nishimura · Y. J. Liu

Thermal analysis of carbon-nanotube composites using a rigid-line inclusion model by the boundary integral equation method

Abstract The boundary integral equation (BIE) method is applied for the thermal analysis of fiber-reinforced composites, particularly the carbon-nanotube (CNT) composites, based on a rigid-line inclusion model. The steady state heat conduction equation is solved using the BIE in a two-dimensional infinite domain containing line inclusions which are assumed to have a much higher thermal conductivity (like CNTs) than that of the host medium. Thus the temperature along the length of a line inclusion can be assumed constant. In this way, each inclusion can be regarded as a "rigid line" (the opposite of a crack) in the medium. It is shown that, like the crack case, the hypersingular (derivative) BIE can be applied to model these rigid lines. The boundary element method (BEM), accelerated with the fast multipole method, is used to solve the established hypersingular BIE. Numerical examples with up to 10,000 rigid lines (with 1,000,000 equations), are successfully solved by the BEM code on a laptop computer. Effective thermal conductivity of fiber-reinforced composites are evaluated using the computed temperature and heat flux fields. These numerical results are compared with the analytical solution for a single inclusion case and with the experimental one reported in the literature for carbon-nanotube composites for multiple inclusion cases. Good agreements are observed in both situations, which clearly demonstrates the potential of the developed approach in large-scale modeling of fiber-reinforced composites, particularly that of the emerging carbon-nanotube composites.

N. Nishimura
Academic Center for Computing and Media Studies,
Kyoto University, Kyoto 606-8501, Japan

Y. J. Liu (✉)
Department of Mechanical, Industrial and Nuclear Engineering,
University of Cincinnati, P.O. Box 210072,
Cincinnati, OH 45221-0072, U.S.A
Tel.: +1-513-5564607
Fax: +1-513-5563390
E-Mail: Yijun.Liu@uc.edu

1 Introduction

Modeling of rigid-line inclusions can find important applications in the analysis of composite materials. For example, the stress distribution and interaction of fibers in a fiber-reinforced composite can be investigated by treating the fibers as rigid-line inclusions. The effective material properties of such composites can also be evaluated using rigid-line models. This rigid-line approximation is valid when the fibers have much higher values of stiffness and/or thermal conductivity compared with those of the matrix. This approximation can significantly reduce the modeling complexity in the analysis without losing much accuracy. In the case of carbon nanotube (CNT)-based composites, the CNTs are in general in a slender shape with very large aspect ratios and have values of both stiffness and thermal conductivity several orders higher than those of a matrix material. For example, the Young's modulus of CNTs is in general greater than 1 TPa, while the thermal conductivity is in the range of 2000–6000 W/m-K at the room temperature (see, e.g., Refs. [1–10]). Thus, the rigid-line approach seems to be especially suitable and promising for large scale modeling and analysis of CNT-based composites using the continuum approach, when the overall (not local) mechanical properties of the composites are to be investigated [11–13].

In the case of the stress analysis of rigid-line inclusions (also called anti-cracks) in an elastic solid, many research results have been reported in the literature. In this analysis, the rigid-line inclusions, representing, for example, fibers in a matrix, are assumed to have no elastic deformations and only have rigid-body motions, that is, three degrees of freedom in two dimensions (2-D)

and six degrees of freedom in three dimensions (3-D). Boundary integral equation (BIE) methods have been found especially suitable for the analysis of rigid-line inclusions, since the counter part of rigid lines, cracks, have been studied intensively by using the BIEs. Many of the results for crack analysis can be extended readily to the analysis of rigid-line inclusions. In the early of 1990's, the group of Hu, Chandra and Huang made considerable contributions to the study of rigid-line inclusions in a matrix using the boundary integral equation method. Some of their work can be found in Refs. [14–18]. In these works, the rigid lines are represented by distributions of tractions along the rigid lines (as compared to distributions of dislocations for cracks) and integral equations are established using the Green's functions. The interactions of rigid lines with cracks and the effects of rigid lines on the effective elastic material properties of a composite were successfully studied using this approach for 2-D models by Hu, Chandra and Huang. Extensive review of the earlier theoretical work on the elasticity study of rigid-line inclusions in a solid can also be found in their papers [14–18]. Recently, there seems to be a renewed interest in the study of rigid-line inclusions using the BIEs. In Ref. [19], Leite, Coda and Venturini reported a 2-D boundary integral equation method coupled with the finite elements that are used to model the elastic bar inclusions in a matrix. These bar inclusions, representing fibers in a matrix, are assumed to be rigid within any cross section of a bar, but can deform along the axial direction of the bar in their models. The displacement and stress fields near the bar inclusions are studied by this approach. In Ref. [20], Dong, Lo and Cheung developed a hypersingular BIE approach for the analysis of interactions of rigid-line inclusions with cracks in a 2-D elastic medium. Stress intensity factors at the two ends of rigid lines are computed with this hypersingular BIE approach and compared with analytical solutions. In all the work mentioned above, only 2-D models with a small number (less than 10) of rigid-line inclusions are considered.

In the case of thermal analysis of rigid-line inclusions in a matrix, there seems to be no research work published for this very important study. For the thermal analysis, a rigid-line inclusion means a one-dimensional line model of a thin, slender inclusion having a constant-temperature distribution (c.f., a rigid-body motion of a rigid line in the elasticity case), assuming that the thermal conductivity (c.f., the stiffness) of the line inclusion is much higher than that of the hosting matrix. In a recent related work, Zhang, Tanaka and Matsumoto [21] studied the heat conduction problem of carbon nanotube composites using 3-D unit-cell models. The boundary node method was employed in which the CNTs are represented by capsule-like voids in the matrix with constant temperature distributions being described on the voids. The boundary node equations are supplemented with additional equations representing the balance of the heat flux for each CNT. Up to two CNTs in a unit cell were studied and good agreement was observed between the simplified model and the full model where the CNTs were modeled as another thin-layer domain. The effectiveness of the CNT in increasing the effective thermal conductivity of the CNT composite is evident from their simulations based on the simplified models.

With the advances of new composites, especially those employing carbon nanotubes as the reinforcing fibers, new modeling approaches that can handle models with large numbers of slender inclusions need to be developed. The rigid-line approach seems to be one of the few feasible approaches with the current computing hardware capabilities. The BIE method (also referred to as boundary element method) based on the Green's functions is a natural way to model the rigid-line inclusions, due to its reduction of the dimension of a problem domain and the high accuracy the integral approach offers. With the development of the fast multipole methods (see, e.g., a recent review [22] and Refs. [23–28]) for solving boundary integral equations, large models with several millions of degrees of freedom can be solved readily on a desktop computer. All these needs in materials research and progresses in numerical methods suggest that the BIE approach for modeling rigid-line inclusions may play a significant role in the analysis of fiber-reinforced composites, such as the CNT-based nanocomposites.

In this paper, a BIE method is developed for the thermal analysis of rigid-line inclusions in a 2-D medium. This mathematical model can represent, for example, composite thin films with long fibers as the reinforcing material. A hypersingular BIE formulation is established that can handle line inclusions with constant temperature distributions. The boundary element method accelerated with the fast multipole method is used to solve the hypersingular BIE. Numerical examples with up to 10,000 rigid lines (with 1,000,000 equations), are successfully solved by the developed BEM code on a laptop computer. Effective thermal conductivity of the composites are evaluated using the computed temperature and heat flux fields. The developed method and code are validated by comparisons with the analytical solution for the case using a single rigid-line inclusion, and with experiments for CNT-based composites for the case using many rigid-line inclusions. Good agreement is observed regarding the trends and values of these results, which clearly demonstrates the potential of the developed BIE approach in the large-scale modeling of fiber-reinforced composites, particularly that of the CNT-based composites.

2 Hypersingular BIE formulation for rigid-line inclusions

The hypersingular BIE for the thermal analysis of a medium containing rigid-line inclusions is derived in this section. Consider the following Laplace equation governing the steady-state heat conduction in a 2-D infinite medium embedded with rigid-line inclusions (Fig. 1):
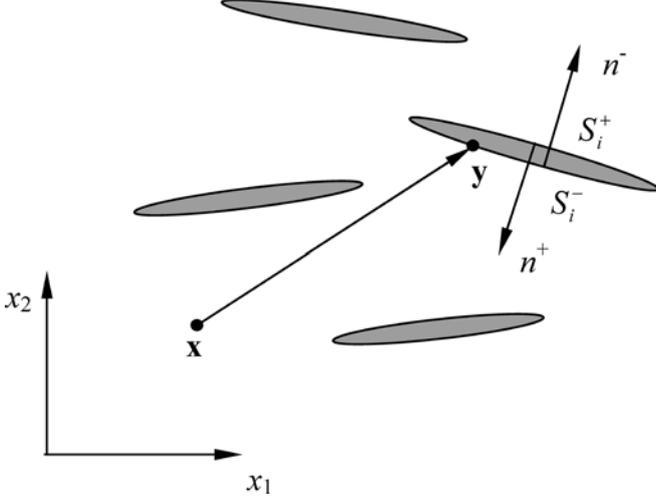
Fig. 1 A 2-D infinite medium embedded with rigid-line inclusions

$$\nabla^2\phi(\mathbf{y}) = 0, \quad \forall \mathbf{y} \in R^2\backslash S \ , \tag{1}$$

under the boundary and regularity conditions:

$$\phi(\mathbf{y}) = \phi_i, \quad \forall \mathbf{y} \in S_i, \ i = 1, 2, \dots \ , \tag{2}$$

$$\int\limits_{S_i^+ \bigcup S_i^-} \frac{\partial\phi}{\partial n}(\mathbf{y})\mathrm{d}S(\mathbf{y}) = 0, \ i = 1, 2, \dots \ , \tag{3}$$

$$\phi(\mathbf{y}) = \phi^\infty(\mathbf{y}), \quad \text{as } |(\mathbf{y})| \to \infty \ , \tag{4}$$

where R^2 is the full 2-D space, ϕ the temperature (potential) field, $S_i^+ \bigcup S_i^-$ the boundary of the i-th rigid line, $S = \bigcup_i (S_i^+ \bigcup S_i^-)$, n the outward normal, ϕ_i an unknown constant temperature value, and ϕ^∞ the undisturbed field (the solution when the rigid-line inclusions are not present).

The solution to the boundary value problem described by Eqs. (1–4) can be written as the following representation integral (see, e.g., Refs. [29–31]):

$$\phi(\mathbf{x}) = \int\limits_S \left[G(\mathbf{x}, \mathbf{y})\frac{\partial\phi}{\partial n}(\mathbf{y}) - \frac{\partial G(\mathbf{x}, \mathbf{y})}{\partial n}\phi(\mathbf{y}) \right]\mathrm{d}S(\mathbf{y})$$
$$+ \phi^\infty(\mathbf{x}), \ \forall \mathbf{x} \in R^2\backslash S \ , \tag{5}$$

where $G(\mathbf{x}, \mathbf{y})$ is the Green's function given by:

$$G(\mathbf{x}, \mathbf{y}) = \frac{1}{2\pi} ln\left(\frac{1}{r}\right) \ , \tag{6}$$

with r being the distance between the source point $\mathbf{x}$ and field point $\mathbf{y}$.

Let $S_i^+ \to S_i^- (\equiv S_i)$ (Fig. 1) for each line inclusion, one has from Eq. (5):

$$\phi(\mathbf{x}) = \sum_i \int\limits_{S_i} G(\mathbf{x}, \mathbf{y})\Delta q(\mathbf{y})\mathrm{d}S(\mathbf{y})$$
$$+ \phi^\infty(\mathbf{x}), \ \forall \mathbf{x} \in R^2\backslash \bigcup_i S_i \ , \tag{7}$$

in which condition (2) has been applied and:

$$\Delta q(\mathbf{y}) = -\frac{\partial\phi(\mathbf{y}^+)}{\partial n} + \frac{\partial\phi(\mathbf{y}^-)}{\partial n}, \ \text{with } n = n^- \ . \tag{8}$$

Letting the source point $\mathbf{x}$ approach the surface S_i from either side of the surface, one obtains the following same equation:

$$\phi_i = \sum_i \int\limits_{S_i} G(\mathbf{x}, \mathbf{y})\Delta q(\mathbf{y})\mathrm{d}S(\mathbf{y})$$
$$+ \phi^\infty(\mathbf{x}), \ \forall \mathbf{x} \in \bigcup_i S_i \ , \tag{9}$$

in which no jump terms arise from the limiting process due to the weak singularity of the kernel. Equation (9) is a weakly-singular BIE for the rigid-line inclusion problems. One can employ this equation to determine $\Delta q(\mathbf{y})$ on each rigid line first and then apply Eq. (7) to compute the $\phi(\mathbf{x})$ inside the domain. To solve Eq. (9), additional equations are needed, since the constant temperature ϕ_i (one value) for each rigid line (on the left-hand side of (Eq. (9)) is also unknown. These additional equations can be obtained by applying Eq. (3) for each rigid line. This approach is feasible (contrary to the crack case where there are not enough equations from Eq. (5)). However, it is difficult to represent $\Delta q(\mathbf{y})$ accurately on each rigid line using the boundary elements, since $\Delta q(\mathbf{y})$ (corresponding to stresses in the elasticity case) has singularity at the two ends of a rigid line (just like the crack case). In addition, in the present work, the fast multipole method will be employed. BIE (9) does not have the diagonal dominance due to the weak singularity of the kernel, which may pose problems for the iterative solvers with the fast multipole method. Therefore, it will be advantageous (as in the crack case) to employ a hypersingular BIE that involves a variable with no singularity over the rigid line, that can satisfy the conditions (1–3) automatically without introducing additional equations, and that can have the diagonal dominance to suite the fast multipole method.

To derive the hypersingular BIE, introduce a "tangential potential" $w(\mathbf{y})$ such that:

$$\Delta q(\mathbf{y}) = \frac{\partial w}{\partial t}(\mathbf{y}), \quad \text{on } S_i, \quad \text{and } w(e_1) = w(e_2) = 0 \ , \tag{10}$$

where e_1 and e_2 are the two end points of the inclusion S_i (see Fig. 2 for the orientation of tangent t with respect to normal n). Then condition (3) is satisfied automatically. Substitution of (10) into Eq. (7) yields:

$$\phi(\mathbf{x}) = \sum_i \int\limits_{S_i} G(\mathbf{x}, \mathbf{y})\frac{\partial w}{\partial t}(\mathbf{y})\mathrm{d}S(\mathbf{y})$$
$$+ \phi^\infty(\mathbf{x}), \ \forall \mathbf{x} \in R^2\backslash \bigcup_i S_i \ ,$$

Applying integration by parts and the conditions in (10) in the above result, one obtains:

$$\phi(\mathbf{x}) = -\sum_i \int\limits_{S_i} \frac{\partial G(\mathbf{x}, \mathbf{y})}{\partial t(\mathbf{y})} w(\mathbf{y})\mathrm{d}S(\mathbf{y})$$
$$+ \phi^\infty(\mathbf{x}), \ \forall \mathbf{x} \in R^2\backslash \bigcup_i S_i \ , \tag{11}$$
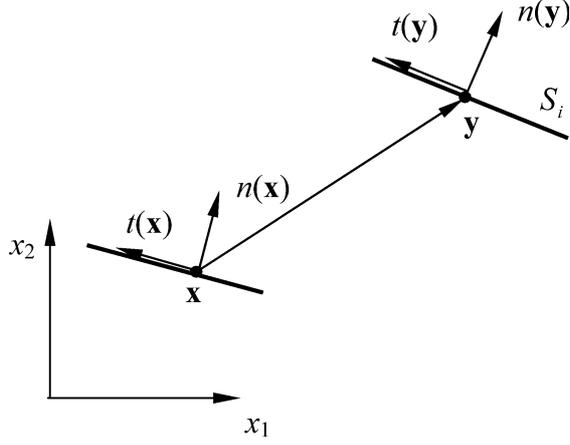
Fig. 2 The normal n and tangent t at the source point $\mathbf{x}$ and field point $\mathbf{y}$

Equation (11) can be applied to compute the temperature field ϕ at any point in the domain once the function w is determined on all the line inclusions.

Placing $\mathbf{x}$ on a rigid line and taking derivative of the above expression with respect to the tangent t at the source point $\mathbf{x}$ (see Fig. 2), one has:

$$0 = -\sum_i \text{f.p.} \int_{S_i} \frac{\partial^2 G(\mathbf{x},\mathbf{y})}{\partial t(\mathbf{x}) \partial t(\mathbf{y})} w(\mathbf{y}) dS(\mathbf{y})$$
$$+ \frac{\partial \phi^\infty(\mathbf{x})}{\partial t(\mathbf{x})}, \quad \forall \mathbf{x} \in \bigcup_i S_i \ , \tag{12}$$

where condition in (2) has been applied again and the integral is a hypersingular one that must be interpreted in the sense of Hadamard finite part (f.p.). It is easy to verify that:

$$\frac{\partial^2 G(\mathbf{x},\mathbf{y})}{\partial t(\mathbf{x}) \partial t(\mathbf{y})} = -\frac{\partial^2 G(\mathbf{x},\mathbf{y})}{\partial n(\mathbf{x}) \partial n(\mathbf{y})} \ ,$$

Thus, Eq. (11) can be rewritten as:

$$0 = \sum_i \text{f.p.} \int_{s_i} \frac{\partial^2 G(\mathbf{x},\mathbf{y})}{\partial n(\mathbf{x}) \partial n(\mathbf{y})} w(\mathbf{y}) dS(\mathbf{y})$$
$$+ \frac{\partial \phi^\infty(\mathbf{x})}{\partial t(\mathbf{x})}, \quad \forall \mathbf{x} \in \bigcup_i S_i \ . \tag{13}$$

This equation is exactly the same hypersingular BIE (except for a different free term) used for crack problems in the potential case (where the normal derivative of ϕ is given, while the difference of ϕ on the two surfaces of a crack is not). The treatment of the hypersingular integral in Eq. (13), which is similar to the 3-D case, can be found in Refs. [26, 28].

The hypersingular BIE (13) is employed to determine the values of the tangential potential w. The temperature field ϕ and its derivatives at any (data collection) point $\mathbf{x}$ can be determined by Eq. (11) and its derivatives once w is known. In this paper, constant boundary elements are used to discretize the hypersingular BIE (13), where one node is placed on each element and the field is assumed to be constant over each element. All the integrals involved are evaluated analytically. This avoids the use of numerical integration and hence guarantees the accuracy in the evaluation of all the integrals when the source point $\mathbf{x}$ is very close to an element of integration (which happens when many inclusions are to be packed closely in a model).

The fast multipole method [22, 26, 28] is employed to accelerate the solution of the boundary element method for solving Eq. (13). In recent years, the fast multipole BEM has been found to be especially good for the analysis of problems with large numbers of cracks and inclusions in both 2-D and 3-D cases (see, e.g., Refs. [23–28]). Using the fast multipole method for the BEM, the solution time of a problem is reduced to order O(N), instead of O(N^2) in the traditional approach (with N being the number of equations). The memory requirement is also reduced since the iterative solver (such as GMRES) does not need to store the entire matrix in the memory. Thus, large models that had to be solved on a supercomputer in the past can now be solved on a laptop computer, as demonstrated in the examples presented in the next section.

3 Numerical examples

The developed BIE code for the analysis of rigid-line inclusions is first validated using a simple test case with one rigid line. Then, the code is applied to study the effects of rigid-line inclusions on the effective thermal conductivity of the resulting composites (or composite thin films in this 2-D situation). All the computations reported in this section were carried out on a laptop PC with a 2.4 GHz CPU, 512 Mb RAM and a 40 Gb hard drive. The largest model with one million equations run for about 4,000 CPU seconds on this PC.

To estimate the effective thermal conductivity of a composite, the temperature and heat flux distributions at some locations, to be called data-collection points (Fig. 3), are computed using Eq. (11) and its derivatives, after the tangential potential w is determined on each rigid line. The effective thermal conductivity of the composite is estimated using the temperature and heat flux results at these data-collection points by the following formula:

$$k_{1(\text{eff})} = -\frac{q_{1(\text{ave})} L}{(\Delta \phi)_{(\text{ave})}} \ , \tag{14}$$

where $k_{1(\text{eff})}$ is the effective thermal conductivity in the x_1 direction, and the averaged fields are obtained by:

$$(\Delta \phi)_{(\text{ave})} = (\phi(x_1 = L))_{(\text{ave})} - (\phi(x_1 = 0))_{(\text{ave})} \ , \tag{15}$$

$$q_{1(\text{ave})} = \lfloor (q_1(x_1 = 0))_{(\text{ave})} + (q_1(x_1 = L))_{(\text{ave})} \rfloor / 2 \ , \tag{16}$$

at the data-collection points, and

$$q_1 = -k_0 \frac{\partial \phi}{\partial x_1} \ , \tag{17}$$
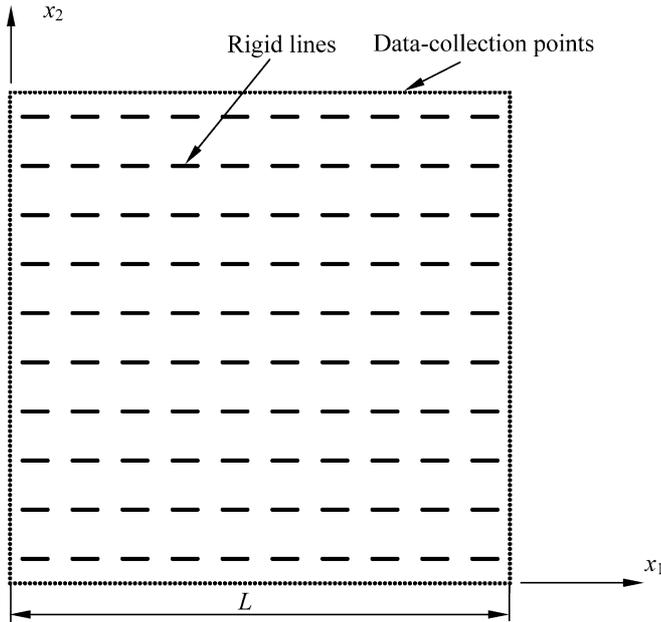
Fig. 3 The infinite domain with rigid lines and the data-collection points

with k_0 being the thermal conductivity of the matrix material (assumed to be isotropic).

3.1 Infinite space with one rigid-line inclusion

The case of a single rigid line, or many well-separated rigid lines, in a 2-D infinite medium is studied first. A far-field (or undisturbed) temperature distribution:

$$\phi^\infty(x_1, x_2) = T_0 x_1 / L \ , \tag{18}$$

is imposed to the model, where T_0 is a constant and L a length dimension (Fig. 3). For a straight rigid-line inclusion along the x_1 axis and centered at the origin, the analytical solution of the tangential potential w is given by (c.f., the crack opening displacement of a crack):

$$w(x_1, 0) = -\frac{2T_0}{L} \sqrt{a^2 - x_1^2} \ , \tag{19}$$

in which a is the half length of the rigid line. Notice that w is dependent on the half length a.

Figure 4 shows the computed tangential potential w for a single rigid-line inclusion aligned with the x_1 axis, with $a = 1$, $T_0 = 1$, and $L = 1$. The numbers of elements are increased from 20, 40, 60 to 100, and the results are compared with the analytical solution given in Eq. (19). Good agreement is achieved. The errors are 3.3% for using 20 elements, 1.7% for 40 elements, 1.1% for 60 elements, and 0.7% for 100 elements. This remaining error may be due to the tip singularity of the field (see, e.g., Refs. [14–16, 20] and the references therein) which can not be represented analytically by the constant elements used in this work. However, this small error is acceptable in the study of estimating the effective thermal conductivity of the medium since the field quantities off the rigid lines (boundaries) will be evaluated by the integral expression (11) and averaged over many data-collection points. Figure 4 suggests that 40 elements per rigid line will be sufficient if the rigid lines are well separated in a model, while 100 elements per rigid line will be needed if many rigid lines are packed closely in a model (see examples in Sect. 3.3). It is also worthwhile to point out that the derivative of w along the rigid-line axis has singularities at the two end points of the rigid line, as shown in Fig. 4. This can cause serious numerical problems should the difference of the flux $\Delta q (= \partial w / \partial t)$
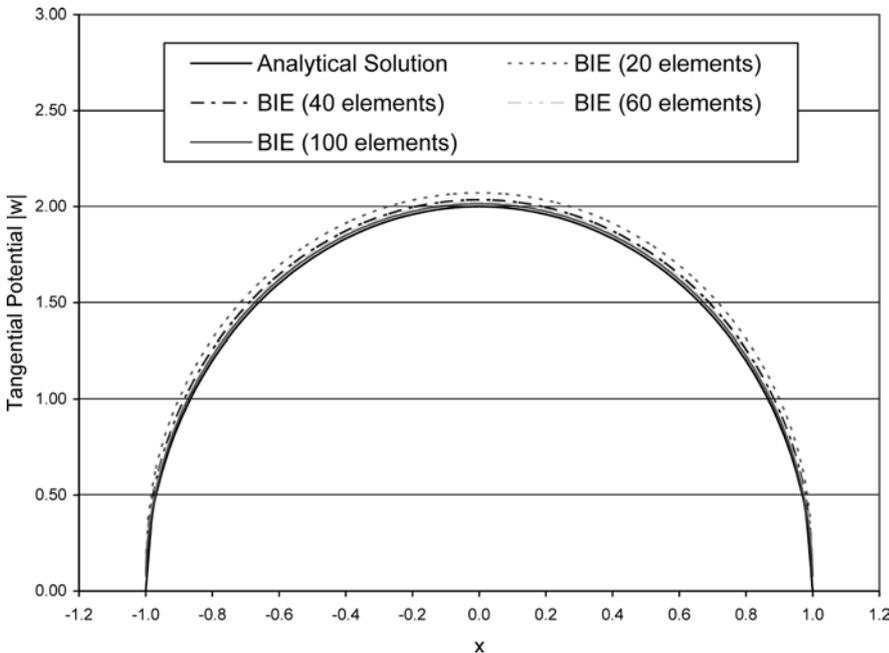
Fig. 4 The computed tangential potential for a single rigid-line inclusion

across a rigid line be used directly in the BIE (i.e., BIE (9)).

3.2 A medium with multiple rigid-line inclusions

An array of 100 (10×10) rigid lines in a medium as arranged in Fig. 3 is studied next. The temperature distribution at 400 data-collection points (which forms a box, starting at $x_1 = 0$ and along the x_1 axis) are computed for different lengths ($2a$) of the rigid lines, under the same far-field temperature distribution given in Eq. (18). The rigid lines are aligned in the x_1 direction and uniformly distributed within a unit square ($L = 1$, Fig. 3). Fourty boundary elements are used for each rigid line, with a total DOF (degrees of freedom) = 4000 for the whole model. A convergence study showed that little improvement in the results can be achieved using more than 40 elements per rigid line in this model.

Figure 5 shows the distribution of the computed relative temperature (the temperature relative to that at $x_1 = x_2 = 0$) along the edges of the box formed by the data-collection points shown in Fig. 3. As the length of the rigid lines increases, the temperature drops along the line at $x_1 = L$ (with data-collection point numbers ranging from 100 to 200). The effectiveness of the rigid lines on enhancing the heat conduction in the medium is obvious. In addition, longer rigid lines are better for the heat conduction in the medium, as expected.

3.3 Estimates of the effective thermal conductivity of composite materials

The effective thermal conductivity of composite materials are estimated next using Eqs. (14–17) and the BIE code developed. In a fiber-reinforced composite material, the fibers can be dispersed randomly in both orientations and distributions, and can be curved and with different lengths. In the models studied here, only the cases with straight, aligned fibers of the same length are considered, which are close to the desired design of a composite. However, the spatial distributions of the fibers are allowed to change randomly, but within their own "territories" (rectangles) to avoid overlapping of the fibers (a "controlled" random distribution).

Figure 6 is a plot for the computed effective thermal conductivity for a composite model with 100 (10×10) rigid lines with an increasing length and packed in a unit square, for both uniform distribution (c.f., Fig. 3) and "controlled" random distribution (a fixed arrangement with varying lengths, c.f., Fig. 7 (a)). The applied far-field temperature is the same as given in Eq. (18). The computed temperature and temperature gradients at the data-collection points on the edges of the square are used to estimate the effective thermal conductivity. It is observed from Fig. 6 that the effective thermal conductivity increases more in the uniform distribution case than in the random distribution case, as the length of the rigid lines (thus the volume fraction) increases. This increase of the effective thermal conductivity follows a nonlinear curve. This phenomenon is consistent with the experimental data reported in Ref. [7], that also shows a nonlinear increase of the thermal conductivity with the increase of the volume fraction for a CNT-filled composite medium (where the ratio of thermal conductivities of the CNT to matrix exceeds 13,800).

Figure 7 shows four different arrays of rigid lines packed in the unit square (where $x = x_1, y = x_2$). The obtained data for the effective thermal conductivity of the composite models are listed in Table 1, which clearly demonstrates the increase of the thermal conductivity of the composites. Even with 100 rigid lines, the effective thermal conductivity is increased by 57% compared with
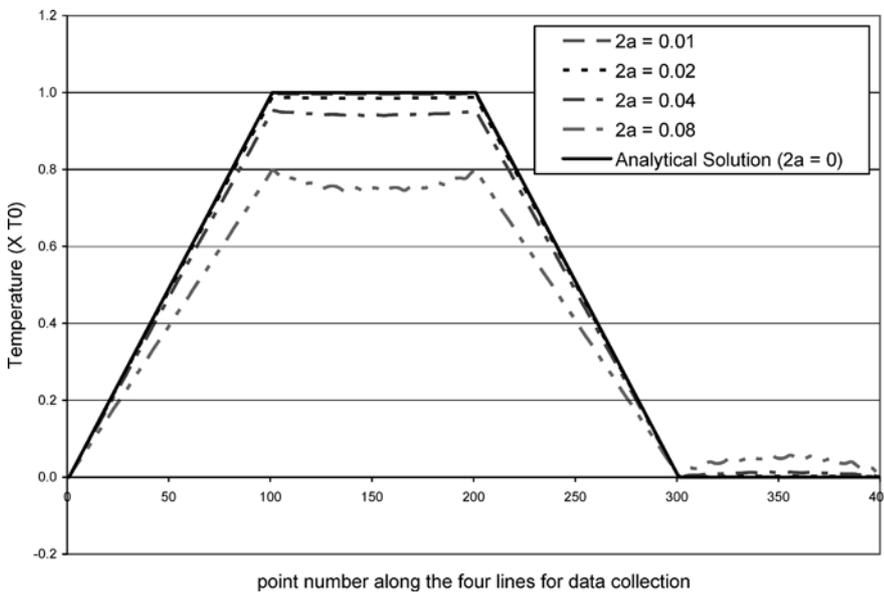
Fig. 5 Computed temperature at the data-collection points for a model with 10×10 aligned and uniformly distributed rigid lines (as shown in Fig. 3)

Fig. 6 Estimated eective thermal conductivity for a composite model with 100 rigid lines (40 elements per line)
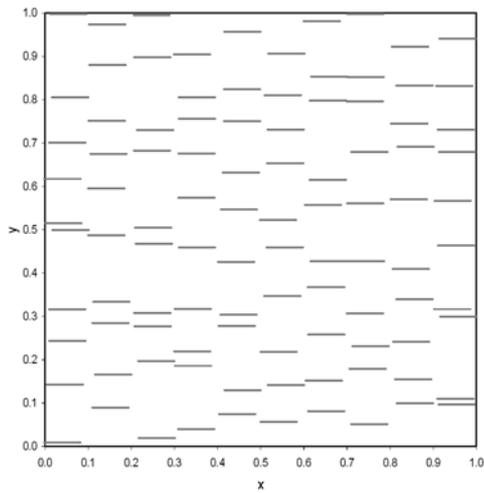
(a) 10X10, 2a = 0.08, DOF = 4,000.
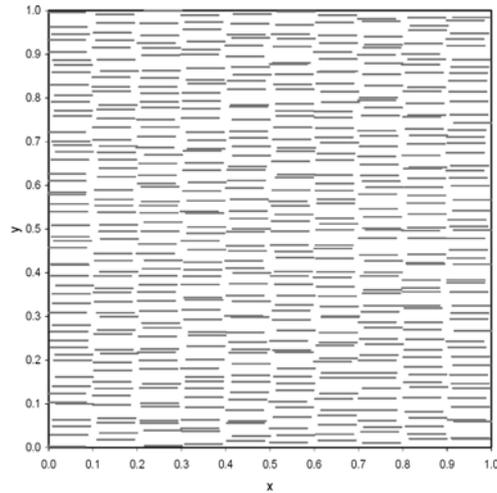
(b) 10X50, 2a = 0.08, DOF = 20,000.
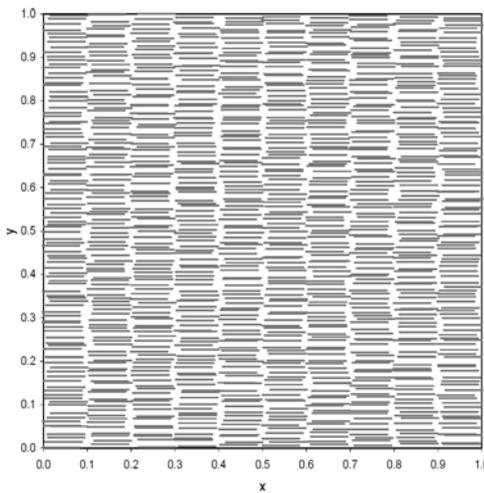
(c) 10X100, 2a = 0.08, DOF = 100,000.
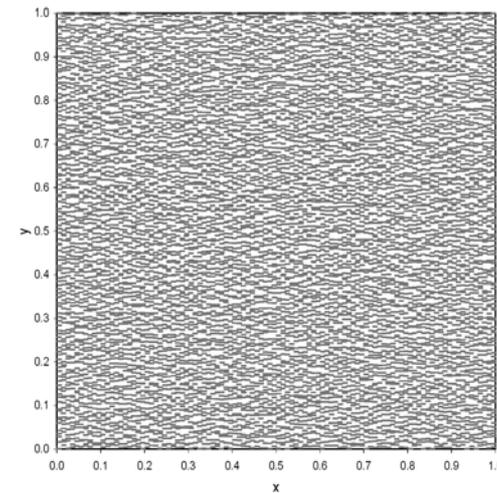
(d) 100X100, 2a = 0.008, DOF = 1,000,000.

Fig. 7 A unit square filled with "randomly" distributed rigid lines with four different densities

Table 1 Estimated effective thermal conductivity for the four composite models shown in Fig. 7.

Note k_0 is the thermal conductivity of the matrix

Model of composites (see Fig. 8)	No. of elements/ line, total DOF	Effective thermal conductivity ($\times k_0$)
(a) 10×10 lines, $2a = 0.08$	40 elements/line, DOF = 4,000	1.5747
(b) 10×50 lines, $2a = 0.08$	40 elements/line, DOF = 20,000	3.3105
(c) 10×100 lines, $2a = 0.08$	100 elements/line, DOF = 100,000	4.4378
(d) 100×100 lines, $2a = 0.008$	100 elements/line, DOF = 1,000,000	1.5493

that of the matrix. With more rigid lines of the same length being added, the increase reach 231% for 500 rigid lines, and 343% for 1,000 rigid lines. However, when the rigid lines are cut into smaller segments (e.g., each rigid line in case (c) is divided into ten smaller lines to obtain case (d)), the effective thermal conductivity is dropped considerably, with the increase at only 56% compared with that of the matrix. Again, this suggests that longer fibers of a high thermal conductivity will have a better thermal enhancement in a composite, as expected. More elements (100 per line) are used for cases (c) and (d), since when more rigid lines are packed in the same area, interactions among them will intensify and the fields will change more rapidly.

Figure 8 is an attempt to directly compare the BIE results of the effective thermal conductivity with the available experimental data reported in Ref. [7]. The measured data for effective thermal conductivity of a medium dispersed with carbon nanotubes for volume fractions up to 1% are provided by Choi, Zhang, et al. in Ref. [7]. However, there are many difficulties in this direct comparison, since the mathematical model based on the continuum assumptions and used for the BIE simulation can not account for many physical phenomena, such as the conditions at the interfaces of the fibers and hosting medium, especially at the nanoscale. There are technical difficulties as well, because the rigid-line model does not even give a volume fraction

readily. Nevertheless, a comparison is presented here for discussions and further investigations. To come up with an equivalent volume fraction for the BIE model, the diameter of the CNT mentioned in Ref. [7], 25 nm, is inferred for the rigid lines. A total of 8,000 (20×400) aligned and uniformly distributed rigid lines are used in a square model with the edge length of 1 mm. The length ($2a$) of the rigid lines is increased from 0.005, 0.01, up to 0.05 mm, which is the observed length of the CNTs for the experiment mentioned in Ref. [7]. In this way, a volume fraction can be determined for the BIE model at each length of the rigid lines, up to 1% volume fraction before the rigid lines connect with each other along the x direction. As shown in Fig. 8, the computed effective thermal conductivity follows the experimental data closely up to volume fraction = 0.4%. Then, the simulation data depart from the experimental ones and increase at a much faster rate. There can be many sources for these differences. First, the BEM model is a 2-D model with aligned rigid-line inclusions, while the experimental one is in 3-D and with randomly distributed and oriented CNTs. Second, the BEM assumes a perfect bonding interface condition between the rigid lines and matrix, while for the experimental case there may exist discontinuities in the temperature and heat flux across the interface between the CNTs and matrix. The comparison here is merely intended to show the trends of the
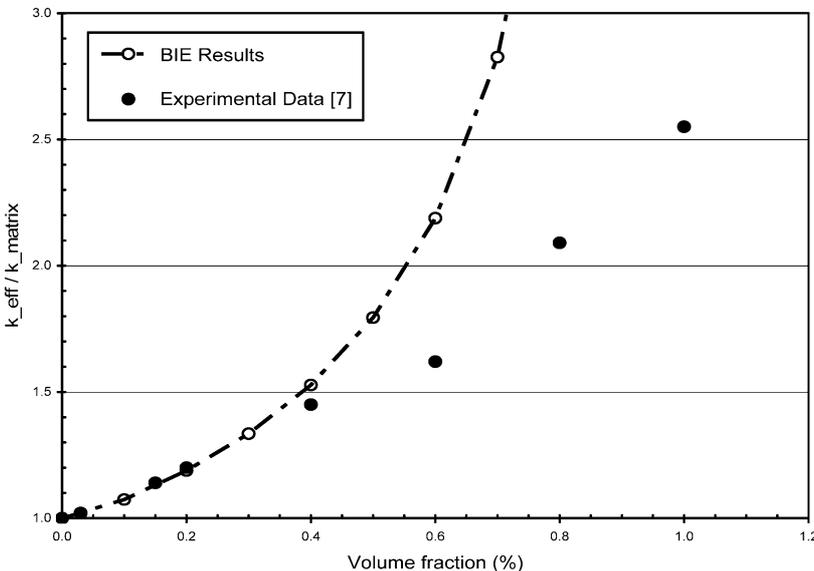
Fig. 8 A direct comparison of the computed eective thermal conductivity by the BIE with the experimental data reported in Ref. [7] for a CNT filled mediu

two approaches. Further investigations are needed and improvements to the simulation models, including a more realistic interface condition, can be made.

4 Discussions

In the convergence tests carried out in this study, it was found out that 100 elements per rigid line are sufficient for obtaining converged results for determining the effective thermal conductivities, even in the case with densely-packed rigid lines. This is true because the fields used for estimating the thermal conductivities are inside the domain, not on the boundaries (rigid lines in this case). If the heat flux, which is the derivative of the tangential potential and singular at the two ends of a rigid line, is to be evaluated right on the rigid lines, then many more elements will definitely be needed.

Higher-order elements can certainly be employed to improve the accuracy and efficiency of the developed BEM code. The constant elements are used in this study because they are the simplest elements that can satisfy the C^1 continuity requirement (at the collocation point) on the density function for a hypersingular BIE, while allowing analytical integrations of all integrals. The latter is crucial for accuracy in solving a problem with many closely packed inclusions. Higher-order elements for hypersingular BIEs are much more involved in either formulations (e.g., variational ones) or implementations. However, improved accuracy and efficiency of the code can be expected from using higher-order elements. A singular element that can capture the tip singularity of the rigid line can also be developed readily with higher-order elements.

The square box, on the four edges of which the data-collection points are located (Fig. 3), can be moved into the region containing the rigid lines. This can avoid the possible boundary effects of the infinite domain model used in this study. However, it was found that the difference in the computed values for the effective thermal conductivity is only about 5% when the box was moved into the region occupied by the rigid lines.

There are some obvious limitations of the developed BIE/BEM approach for the thermal analysis of fiber-reinforced composites, although it has been shown to be very promising in some special cases. One limitation is that this rigid-inclusion approach cannot account for the effect of the ratio of thermal conductivities of the fiber to matrix, which is assumed as infinity for any matrix material. It may also be difficult to generalize this approach to three dimensions, since the boundary integral equations will be reduced to a line in 3-D space that may cause some additional singularity problems. A more general approach that treats the slender rigid inclusions as ones with finite volumes may be needed in 3-D cases.

Further validations of the rigid-line approach for analyzing composite materials should be pursued by comparing with new analytical and experimental results. If this approach is valid, the hypersingular BIE formulation can be extended readily to handle finite domain problems, periodic boundary conditions, 3-D thermal analysis, and 2-D and 3-D elasticity problems.

5 Conclusion

A hypersingular BIE formulation is developed in this paper for solving heat conduction problems in a 2-D infinite medium embedded with many rigid-line inclusions that can be treated as having constant temperature distributions. The hypersingular BIE is solved using boundary element method and the solution is accelerated by the fast multipole method. The developed code is validated by using analytical solutions for single rigid-line case and by comparing with the experimental data on carbon nanotube composites for multiple rigid-line cases. The effective thermal conductivity results computed by the BEM code at lower volume fraction ratios follow that of the experimental one, although the two deviate at higher volume fractions. This deviation may be caused by the interface conditions and other limitations in the mathematical model used in the BIE formulation. The developed code is very efficient and accurate for large scale analysis of composites reinforced with fibers that have much higher thermal conductivities. Up to 10,000 rigid lines (with DOF = 1,000,000) are modeled using the BEM code on a laptop computer. All these results clearly demonstrate the potential of the developed BIE approach in large-scale modeling of fiber-reinforced composites, including possibly the carbon nanotube composites.

References

1. Thostenson ET, Ren ZF, Chou T-W (2001) Advances in the science and technology of carbon nanotubes and their composites: a review. Comput. Sci. Technol. 61: 1899–1912
2. Ruoff RS, Lorents DC (1995) Mechanical and thermal properties of carbon nanotubes. Carbon 33: 925–930
3. Hone J, Whitney M, Piskoti C et al (1999) Thermal conductivity of single-walled carbon nanotubes. Phys. Rev. B 59: 2514–2516
4. Yi W, Lu L, Dian-lin Z et al (1999) Linear specific heat of carbon nanotubes. Phys. Rev. B 59: 9015-9018
5. Hone J, Llaguno MC, Nemes NM et al (2000) Electrical and thermal transport properties of magnetically aligned single wall carbon nanotube films. Appl. Phys. Lett. 77: 666–668
6. Berber S, Kwon Y-K, Tománek D (2000) Unusually high thermal conductivity of carbon nanotubes. Phys. Rev. Lett. 84: 4613–4616
7. Choi SUS, Zhang ZG, Yu W et al (2001) Anomalous thermal conductivity enhancement in nanotube suspensions. Appl. Phy. Lett. 79: 2252–2254
8. Kim P, Shi L, Majumdar A et al (2001) Thermal transport measurements of individual multiwalled nanotubes. Phys. Rev. Lett. 87: 215502

9. Biercuk MJ, Llaguno MC, Radosavljevic M et al (2002) Carbon nanotube composites for thermal management. Appl. Phys. Lett. 80: 2767–2769
10. Hone J, Llaguno MC, Biercuk MJ et al (2002) Thermal properties of carbon nanotubes and nanotube-based materials. Appl. Phys. A 74: 339–343
11. Liu YJ, Chen XL (2003) Continuum models of carbon nanotube-based composites using the boundary element method. Electron. J. Boundary Elem. 1: 316–335
12. Liu YJ, Chen XL (2003) Evaluations of the effective materials properties of carbon nanotube-based composites using a nanoscale representative volume element. Mech. Mater. 35: 69–81
13. Chen XL, Liu YJ (2004) Square representative volume elements for evaluating the effective material properties of carbon nanotube-based composites. Comput. Mater. Sci. 29: 1–11
14. Hu KX, Chandra A (1993) Interactions among general systems of cracks and anticracks-an integral-equation approach. J. Appl. Mech 60: 920–928
15. Hu KX, Huang Y (1993) A microcracked solid reinforced by rigid-line fibers. Comput. Sci. Technol. 49: 145–151
16. Hu KX, Chandra A, Huang Y (1994) On crack, rigid-line fiber, and interface interactions. Mech. Mater. 19: 15–28
17. Chandra A, Huang Y, Wei X et al (1995) A hybrid micro-macro BEM formulation for micro-crack clusters in elastic components. Int. J. Numer. Meth. Eng. 38: 1215–1236
18. Huang Y, Hu KX, Chandra A (1995) Stiffness evaluation for solids containing dilute distributions of inclusions and microcracks. J. Appl. Mech. 62: 71–77
19. Leite LGS, Coda HB, Venturini WS (2003) Two-dimensional solids reinforced by thin bars using the boundary element method. Eng. Anal. Boundary Elem. 27: 193–201
20. Dong CY, Lo SH, Cheung YK (2003) Interaction between cracks and rigid-line inclusions by an integral equation approach. Comput. Mech. 31: 238–252
21. Zhang J, Tanaka M, Matsumoto T (2004) A simplified approach for heat conduction analysis of CNT-based nano-composites. Comput. Meth. Appl. Mech. Eng. (to appear)
22. Nishimura N (2002) Fast multipole accelerated boundary integral equation methods. Appl. Mech. Rev. 55: 299–324
23. Peirce AP, Napier JAL (1995) A spectral multipole method for efficient solution of large-scale boundary element models in elastostatics. Int. J. Numer. Meth. Eng. 38: 4009–4034
24. Gomez JE, Power H (1997) A multipole direct and indirect BEM for 2D cavity flow at low Reynolds number. Eng. Anal. Boundary Elem. 19: 17–31
25. Fu Y, Klimkowski KJ, Rodin GJ et al (1998) A fast solution method for three-dimensional many-particle problems of linear elasticity. Int. J. Numer. Meth. Eng. 42: 1215–1229
26. Nishimura N, Yoshida K, Kobayashi S (1999) A fast multipole boundary integral equation method for crack problems in 3D. Eng. Anal. Boundary Elem. 23: 97–105
27. Mammoli AA, Ingber MS (1999) Stokes flow around cylinders in a bounded two-dimensional domain using multipole-accelerated boundary element methods. Int. J. Numer. Meth. Eng. 44: 897–917
28. Yoshida K, Nishimura N, Kobayashi S (2001) Application of new fast multipole boundary integral equation method to crack problems in 3D. Eng. Anal. Boundary Elem. 25: 239–247
29. Banerjee PK (1994) The boundary element methods in engineering, 2nd edn. McGraw-Hill, New York
30. Brebbia CA, Dominguez J (1989) Boundary elements - an introductory course. McGraw-Hill, New York
31. Kane JH (1994) Boundary element analysis in engineering continuum mechanics. Prentice Hall, Englewood Cliffs